CORE

Metadata, citation and similar papers at core.ac.uk

Provided by University of Bath Research Portal

UNIVERSITY OF BATH

Citation for published version:
Matias, A, Blenkinsopp, CE & Masselink, G 2014, 'Detailed investigation of overwash on a gravel barrier', Marine Geology, vol. 350, pp. 27-38. https://doi.org/10.1016/j.margeo.2014.01.009

DOI:
10.1016/j.margeo.2014.01.009

Publication date:
2014

Document Version
Peer reviewed version

Link to publication

University of Bath

General rights
Copyright and moral rights for the publications made accessible in the public portal are retained by the authors and/or other copyright owners and it is a condition of accessing publications that users recognise and abide by the legal requirements associated with these rights.

Take down policy
If you believe that this document breaches copyright please contact us providing details, and we will remove access to the work immediately and investigate your claim.

Download date: 13. May. 2019

DETAILED INVESTIGATION OF OVERWASH ON A GRAVEL BARRIER

Ana Matias[1], Chris E Blenkinsopp[2], Gerd Masselink[3]

[1] CIMA-Universidade do Algarve, 8000 Faro, Portugal, ammatias@ualg.pt

[2]Department of Architecture and Civil Engineering, University of Bath, Bath, BA2 7AY, United Kingdom, c.blenkinsopp@bath.ac.uk

[3]School of Marine Science and Engineering, University of Plymouth, PL4 8AA, U.K., g.masselink@plymouth.ac.uk

Abstract

This paper uses results obtained from a prototype-scale experiment (Barrier Dynamics Experiment; BARDEX) undertaken in the Delta flume, the Netherlands, to investigate overwash hydraulics and morphodynamics of a prototype gravel barrier. Gravel barrier behaviour depends upon a number of factors, including sediment properties (porosity, permeability, grain-size) and wave climate. Since overwash processes are known to control short-term gravel barrier dynamics and long-term barrier migration, a detailed quantification of overwash flow properties and induced bed-changes is crucial. Overwash hydrodynamics of the prototype gravel barrier focused on the flow velocity, depth and discharge over the barrier crest, and the overwash flow progression across and the infiltration through the barrier. During the BARDEX experiment, overwash peak depth (0.77 m), velocity (5 m s^{-1}) and discharge (max. 6 m^3 m^{-1}) were high, especially considering the relatively modest wave energy (significant wave height = 0.8 m). Conversely to schemes found in the literature, average flow depth did not linearly decrease across the barrier; rather, it was characterised by a sudden decrease at the crest, a milder decrease at the barrier top and then propagation as a shallow water lens over the backbarrier. The barrier morphological evolution was analysed over a series of 15-min experimental runs and at the timescale of individual overwash events. Overall, the morphological variation did not result from an accumulation of many small consistently erosive or accretionary events, but rather the mean bed elevation change per event was quite large (10 mm) and the overall morphology change occurred due to a small imbalance in the number of erosive and accretionary events at each location. Two relationships between overwash hydrodynamic variables were deduced from results: (1) between overwash flow depth and velocity a power-type relation was obtained; and (2) a linear relation was observed between overwash flow depth and maximum overwash intrusion distance across the barrier top (i.e. overwash intrusion). Findings from this study are useful to enhance the knowledge of overwash processes and also have practical applications. On the one hand, results shown here can be use for the validation of overwash predictive models, and additionally, the simple empirical relations deduced from the dataset can be used by coastal managers to estimate overwash intrusion distance, which in turn can assist in the location of areas under risk of overwash and breaching.

Key-words: BARDEX; storm; bed-level sensors; gravel; barrier; coastal hazards

1. INTRODUCTION

Gravel beaches are widespread on the wave-dominated coastlines of Northern Europe, Canada, USA, Japan, New Zealand and Latin America (Buscombe and Masselink, 2006), and develop in a variety of settings where sediment supply and wave energy favour the accumulation of coarse sediments in the shore zone (Orford et al., 2002). Overwash plays an important role in the evolution of gravel barrier beaches causing them to migrate inland over time by the 'rollover' mechanism (e.g., Orford and Carter, 1982; Carter and Orford, 1993). This mechanism involves onshore-directed sediment transport driven by storm waves through erosion from the front of the barrier, transfer across the barrier crest and deposition at the back of the barrier in the form of washover deposits. By controlling the rate and spatial pattern of gravel barrier rollover, storm waves have been regarded as driving short-term (annual to decadal) gravel barrier migration (Orford et al., 1995). Overwash can also contribute to other patterns of gravel barrier evolution, such as breaching (Bray and Duane, 2001), barrier breakdown (Pye and Blott, 2009), outlet formation (Hart, 2007) and outlet closure (Orford et al., 1988).

Despite the importance of overwash in determining the dynamic behaviour of gravel beaches, field measurements of overwash are scarce. Important field studies on this subject are reported by Orford et al. (1999), Lorang (2002), Orford et al. (2003) and Bradbury et al. (2005), and in the laboratory by Obhrai et al. (2008). Overwash mainly occurs during storms and accurate field measurements are therefore hazardous and difficult to obtain. Overwash sediment transport in sandy beaches has been measured using pre- and post-storm surveys (e.g., Guillén et al., 1994; Stone et al., 2004), and evaluated with ground photographs and vertical or oblique aerial photographs (e.g., Rodríguez et al., 1994; Cleary et al., 2001). In-situ measurements of gravel barrier overwash sediment transport are very hard to obtain, and are potentially hazardous to people and equipment. Therefore, large-scale flume experiments can provide a valuable complement to field datasets. Although many laboratory experiments have been conducted of sediment transport in the swash or surf zone, only a handful of experiments on overwash have been conducted (Hancock and Kobayashi, 1994; Obhrai et al., 2008; Donnelly, 2008, Alessandro et al., 2010; Kobayashi et al., 2010; Park and Edge, 2010; Figlus et al., 2011), including the Barrier Dynamics Experiment (BARDEX) reported here (Williams et al., 2012). During BARDEX, overwash was simulated with waves that reached 1.0 m at breaking (Matias et al., 2012) and thus were significantly larger than those used in previous laboratory experiments, where wave heights were 0.14–0.33 m. Details about overwash thresholds based on the BARDEX experiment can be found in Matias et al. (2012).

In this work, the overwash simulations completed in Test Series E of the BARDEX experiment (Williams et al., 2012; Matias et al., 2012) are described. Results are presented from two perspectives: (1) the Eulerian perspective where overwash hydraulic variables and associated morphological changes are measured at the barrier crest, which represents the location that defines the transformation from swash to overwash; and (2) the Lagrangian perspective where high-intensity overwash flows and barrier properties are measured across the barrier. To collect data on overwash characteristics and bed changes, a large array of acoustic bed-level-sensors was deployed to collect bed/water surface elevation data at 4 Hz (cf., Turner et al., 2008). The obtained high-frequency data allowed overwash to be analysed on an event-by-event scale to provide valuable insight into overwash behaviour over a gravel barrier. The primary objectives of this paper are to: (1) provide a data-set of overwash hydraulics on gravel barriers; (2) improve and develop empirical relations between key parameters of overwash flow; and (3) gain insight about how overwash evolves across the backbarrier.

2. EXPERIMENTAL SETUP AND METHODS

Experiments to study gravel barrier overwash were undertaken at proto-type scale in the Delta Flume (The Netherlands) during the BARDEX project (Williams et al., 2012). A gravel barrier (35 m long, 5 m wide and 4 m high) composed of sub-rounded gravel ($D = 11$ mm) was constructed in the flume with the mid-barrier crest located at a distance of 95 m from the wave paddle (Figure 1). The beach profile used at the BARDEX experiment was loosely based on Slapton Sands, Devon, England (Austin and Masselink, 2006).

Overwash was studied by exposing the barrier to variable wave and water-level (h_s) conditions (Test Series E1 to E10; cf. Matias et al., 2012); however, for the purpose of this study, only Test Series E10 will be considered because only during this series did frequent backbarrier overwash occur. Test series E10 consisted of eleven 15-min runs in which the water level ($h_s = 3.75$ m), peak wave period ($T_p = 8$ s), significant wave height ($H_s = 0.8$ m) and wave sequence were kept constant to study the behaviour of the barrier under fully-developed overwash conditions. All wave conditions conformed to a JONSWAP spectrum, specified by H_s and T_p.

Barrier morphology was surveyed before and after each run using a roller and actuator which followed the bed profile from an overhead carriage (Figure 1d). The sub-aerial barrier was monitored continuously at 4 Hz using acoustic bed-level sensors (BLS) deployed at 0.5-m spacing (Figure 1e) and approximately 1 m above the bed. These sensors are described in detail in Turner et al. (2008) and were also used by Masselink and Turner (2012) to investigate swash dynamics during BARDEX non-overwash runs. When mounted perpendicular to the bed, the sensors use the time of flight of the reflected signal to obtain non-intrusive Eulerian measurements, with an accuracy of c. 1 mm of the vertical distance to the closest target: the sand level when the bed is “dry”, and the water level when the bed is submerged (Blenkinsopp et al., 2011). A more detailed analysis of BLS data was undertaken for Test Series E10A, E10B and E10C because during those series full overwash and significant deposition occurred on the sub-aerial back-barrier where the BLS were located.

In this study, an overwash event is defined as a single passage of water above the barrier crest; therefore, during the test runs a number of overwash events are recorded at each BLS position. BLS records were pre-processed to separate overwash events and bed-level events, which are measured by the variation in bed elevation before and after the overwash event. For all BLS positioned landward of the beach (BLS32 to BLS 44; Figure 1), every overwash event was identified and isolated. For each overwash event, maximum and average depth, skewness of the water depth distribution and duration of the event were computed.

Based on various morphologic and hydrodynamic parameters, Matias et al. (2012) defined the Overwash Potential (*OP*, equation 1) as a parameter for quantifying the likelihood of overwash, as well as providing an estimate of the overwash water level relative to the barrier crest elevation:

$$OP = [1.1\ (0.35 \tan\beta\ (H_0 L_0)^{0.5} + ([H_0 L_0 (0.563 (\tan\beta)^2 + 0.004)]^{0.5}/2))] + \eta - h_c \quad (1)$$

where $\tan\beta$ is beach slope, H_0 is offshore wave height, L_0 is the offshore wave length, η is the sea level, including astronomical tides and storm surge, and h_c is the barrier crest elevation. The first term of the equation (in square brackets) is the 2% exceedence for the vertical runup predicted by Stockdon et al. (2006). The position and elevation of the barrier crest were determined at the end of the runs, whereby the crest was defined as the location of the profile with the maximum elevation. Beach slope was calculated for the barrier section between mean water level and the top of the beach, where a break in slope was typically observed.

Overwash velocity was calculated following two methods: leading edge and continuity. The leading edge velocity represents the velocity obtained using the time delay between the leading edge of the overwash water between two BLS positions. Because overwash leading edge velocities can be very fast (> 5 m s^{-1}; Matias et al., 2010) and the BLS sensors record at 4 Hz and are spaced at 0.5 m, the leading edge of the overwash often arrives at two successive BLS positions at the same time. Therefore, the leading edge velocity at the crest was computed between BLS30 and BLS33 (before and after the crest position, 1.5 m apart; Figure 1) to obtain an average value for the barrier crest area. The second methodological adjustment is the use of the interpolated timing of water depth = 0.02 m. The definition of 2 cm as the leading edge is somewhat arbitrary; however, this water depth has been used in coastal engineering applications (e.g., Pullen et al., 2007). Alternative measurements of the velocity close to the overwash leading edge were obtained using the volume continuity method described in Blenkinsopp et al.

(2010). In brief, this technique computes a depth-averaged flow velocity based on the local depth and the rate of change of flow volume landward of the point of interest. Obtaining Eulerian estimates of the depth-averaged flow velocity throughout the duration of each overwash event using continuity requires the assumption that there is no infiltration into the bed. This assumption is clearly invalid when considering a gravel barrier beach and as such the technique has only been used to obtain initial flow velocities immediately after arrival of the overwash leading edge when infiltration is expected to be limited.

The maximum distance across the barrier top and backbarrier that overwash water reaches inland is here termed overwash intrusion, and was calculated for every overwash event. Exact overwash intrusion is impossible to measure with sensors at discrete locations, as intrusion is likely to be located somewhere between two consecutive BLS. Therefore, intrusion was interpolated using the overwash depth progression over the last two sensors. The distribution of overwash intrusions is truncated by the backbarrier lagoon and the maximum distance is 9.8 m.

Overwash discharge was computed for all overwash events using the average depth and the depth-averaged velocity, derived using the continuity velocity method, for each BLS position. The infiltration volume was computed by subtracting the discharge volumes between two consecutive sensor positions.

3. MORPHOLOGICAL DEVELOPMENT

During Test Series E10 the morphological changes of the cross-shore profile were similar (Figure 1e). The beach was eroded and became flatter, while the barrier elevation of the crest decreased and its position migrated lagoonward. The barrier eroded on the seaward side and accreted on the lagoon side, and the steep rear-side of the barrier was displaced lagoonward. Thus, during overwash the sediment was eroded from the seaward side of the barrier, transported to the back-barrier region and was deposited both in the sub-aerial and submerged part of the barrier lagoon margin. These deposits created back-barrier slope instabilities which periodically failed and avalanched down the submerged rear-side of the barrier forming a steep prograding surface approximately parallel to the original slope. This test demonstrated the importance of the lagoon water level in controlling the geometry of the back-barrier deposit, particularly at the interception between the subaerial backbarrier deposits and below the lagoon water level. The rate of barrier lowering and widening was relatively constant (c. 7 mm min^{-1}) during Test Series E10 (Figure 1e) and the average sediment transport rate across the barrier crest was 0.1 $m^3m^{-1}min^{-1}$. The volume of sediment transported over the barrier crest was similar for all runs (between 1.1 and 1.8 m^3m^{-1}, with an average of 1.3 m^3 m^{-1}). By the end of Test Series E10, the volume of the washover deposit had increased by 13 m^3 m^{-1}. Approximately 68% of the washover sediment originated from the beachface, with the remaining 32% coming from sediments in the crest region that were deposited by overwash in the earlier test stages of Test Series E10.

Despite hydrodynamic conditions being kept the same, overwash during Test series E10 resulted in a progressive reduction of the barrier crest height, which in turn, increased the likelihood of overwash. This can be summarized in a variation of the Overwash Potential (OP, equation 1, Table 1) which is defined as the difference between the runup elevation and the barrier crest elevation. At the beginning of Test Series E10, OP = 0.75 m, but a decrease to 0.56 m was noticed on the second run because of a significant reduction in beach slope (from 0.20 to 0.16, Table 1), thus reducing the elevation of wave runup. This beach slope variation acts as a negative feedback process by which the variation in beach slope retards the occurrence of overwash. However, as the barrier crest height reduces, and the beach slope compensation is insufficient, OP increases (from 0.56 m in E10B to 0.63 m in E10D to 0.71 m in E10G, Table 1). During Test Series E10, overwash frequency progressively increased due to positive feedback, driven by barrier crest lowering, until the barrier became permanently inundated and the experiment was terminated. Although a corresponding increase in sediment transport would be expected during barrier crest lowering, the rate of morphological change did not increase (Figure 1e). This is attributed to increased dissipation of overwash flow on the flatter back-barrier, promoting deposition, and a reduction in the beachface gradient, enhancing wave dissipation at the front of the barrier.

During the latter runs of the E10 test series, the barrier crest was almost continuously submerged and the backbarrier displaced lagoonward, in part beyond the furthest BLS (BLS 45, Figure 1e). Therefore, a more detailed analysis of overwash dynamics was only possible for the earlier runs, and only runs E10A, E10B and E10C are discussed hereafter.

4. OVERWASH OF THE CREST FROM AN EULERIAN PERSPECTIVE

4.1. Overwash frequency and depth

Figure 2 shows time series of overwash during runs E10A – E10C. Note that due to the identical wave forcing for each of the test runs, the overwash sequence also looks very similar (refer to the pause in overwash towards the end of the test around 17:11). During runs E10A, E10B and E10C, 53, 53 and 62 overwash events were measured, respectively. Therefore, mean overwash frequency was 0.06 Hz, 0.06 Hz and 0.07 Hz, for E10A, E10B and E10C, respectively, which corresponds to a mean overwash period between 14 and 17 s. During Test Series E10 the waves had a significant wave height of 0.8 m and peak period of 8 s; therefore, approximately 50% of waves generated overwash flows. The average duration of overwash events over the barrier crest was between 3.3 s and 3.5 s, with longer overwash durations at the crest generally coinciding with the deeper flows . Nevertheless, the longest overwash over the crest lasted for 6.75 s, but its maximum water depth over the crest was only 26 cm. This was one of the few situations were two swash events interacted to produce a single, double-peaked overwash. Maximum overwash depth over the crest was 77 cm (Table 2), recorded during E10C, while average overwash depth was only about 10 cm, for all runs. Generally, overwash events are characterised by a peak in the water depth closely following arrival of the leading edge, followed by a long shallow 'tail' (see overwash 13 in Figure 3, as an example). The positive skewness of the overwash depth distribution of 0.5 and 0.3 during runs E10A and E10B (Table 2) reflects this shape. The more symmetrical overwash depth distributions during run E10C, characterised by a skewness of only -0.04, is ascribed to the lower barrier crest causing the overwash events to be more resemblant of propagating waves.

In the absence of field measurements, one way to infer overwash depth is through the Overwash Potential (*OP*, Table 1). For runs E10A, E10B, and E10C, the calculated values of *OP* were 0.75 m, 0.56 m, and 0.59 m, respectively. The same statistics were applied to overwash depth to compute the 2% exceedance overwash peak depth ($h_{2\%}$). For E10A, E10B, E10C h_2 was 0.60 m, 0.68 m, and 0.59 m, respectively. Although some non-systematic differences are noticed between *OP* estimates and depth measurements, the range of values is close (60-70 cm), which implies that *OP* can provide rough estimates of maximum overwash depth at the crest.

4.2. Overwash velocity

Overwash velocities over the crest were computed using both the continuity of flow volume method (referred to as 'continuity velocities') and the leading edge method (referred to as 'leading edge velocities'). Calculated velocities compare fairly well in general; however, maximum continuity velocity was 5 ms^{-1}, whereas leading edge velocity can have extremely high velocities that can attain up to 10 ms^{-1} (Figure 4). Mean continuity velocities are also smaller (2.6 ms^{-1}, 2.7 ms^{-1}, and 2.5 ms^{-1}, for E10A, E10B, and E10C, respectively) than mean leading edge velocities (3.0 ms^{-1}, 3.6 ms^{-1}, and 3.0 ms^{-1}, for E10A, E10B, and E10C, respectively). The average difference between the velocities computed with both methods is acceptable (0.5 ms^{-1}); however, individual differences can be much higher (>6 ms^{-1}; Figure 4). On the one hand, the leading edge method is more easily applicable as it can be applied using remote sensing techniques such as video; however, velocities as high as 10 ms^{-1} are only representative of the leading edge of the moving water, which is moving faster than the fluid behind it (as it has been considered for swash movement, e.g., Shen and Meyer, 1963). Accordingly, leading edge velocities are not considered adequate for the computation of other variables such as overwash discharge and infiltration rate. The reason that these velocities are very different is related to the specific nature of water passage over the crest of steep beaches, which are similar to seawalls. For coastal engineering purposes, the way water overtops coastal structures is defined as either ‘white water’ or ‘green water’ (Pullen et al., 2007). In the ‘green water’ overtopping case there is a continuous sheet of water passing over the crest; in cases where the structures are vertical, the wave may impact against the wall and send a vertical plume of water against the crest (Pullen et al., 2007). In the case of gravel barriers, the beach slope is very steep and the visual observation of overtopping at the crest is such that the water is projected as a mixture of ‘green water’ and ‘white water’. This was also observed in the field by Lorang (2002). Accordingly, the leading edge reaches several measurement points almost simultaneously, which results in extremely high leading edge velocities. However, the continuity method integrates the entire water column passing below each sensor, and therefore minimizes the ‘white water’ effect. Finally, one factor that should be taken into account is the equipment sampling frequency. This effect was somewhat minimized by methodological adjustments, but still the slow sampling rate may have contributed to some inaccuracy in this method.

BARDEX overwash average velocities at the crest were generally of the same order of magnitude as overwash velocity on sandy barriers (around 2 ms^{-1}) obtained from the literature regardless of the different methods used and the diverse geographical and oceanographic conditions. Leatherman (1977) obtained a mean overwash flow velocity of 1.95 ms^{-1} in Assateague Island (U.S.A.); Leatherman and Zaremba (1987) measured 0.5–2.0 ms^{-1} overwash flow velocities at Nauset Spit

(U.S.A.); a maximum of 1.5 ms^{-1} was the overwash flow through the Trabucador Bar (Spain; Guillén et al., 1994); mean velocities of 2.0 ms^{-1} were obtained by Holland et al. (1991) at the Isles Dernieres (U.S.A.); Bray and Carter (1992) measured overwash flow velocities between 1 and 3 ms^{-1} at a barrier in Lake Erie (U.S.A.).; and Matias et al. (2010) measured average velocities of 2.2–2.3 ms^{-1} for non-storm overwash on Barreta Island (Portugal). As for experimental studies in flumes, several overwash experiments have been undertaken (e.g., Hancock and Kobayashi, 1994; Bradbury and Powell, 1992; Baldock et al., 2005; Alessandro et al., 2010; Tinh et al., 2010), but published overwash velocities at crest are limited. Srinivas et al. (1992) measured 0.8–1.2 ms^{-1} overwash velocity over a sandy barrier; Schüttrumpf and Oumeraci (2005) measured up to 0.7 ms^{-1} overtopping velocity over an impermeable dike; and Donnelly (2008) measured bore front velocities smaller than 1.5 ms^{-1} on a sandy barrier. BARDEX maximum overwash velocities (up to 5 ms^{-1} with continuity method and 10 ms^{-1} with leading edge method) are significantly higher than those found in the literature for both laboratory and field experiments. There have been measures of tsunami inundation velocities reaching 8 to 11 ms^{-1} but those were from much deeper flows (e.g. Matsutomi et al., 2010, Jaffe et al., 2011). The maximum leading edge velocity measured by Holland et al. (1991) was 2.9 ms^{-1} whereas by Matias et al. (2010) recorded velocities up to 5.7 ms^{-1}. There are a number of potential explanations for this, including differences in the barrier geometry, wave and water level conditions, methods of data collection and barrier sediments (i.e., sand versus gravel). Probably one of the most important factors is the BARDEX beach steepness and the narrowness of the barrier which promote the occurrence of very energetic swash and overwash.

About 95% of all overwash events measured during the BARDEX experiment (168 events) were supercritical flows with average Froude number of 2. These data also showed that there is a relation between leading edge velocity and depth at crest (Figure 5). This relation can be described in two forms: analytical and empirical. The analytical form uses a classical dam break equation, which has also been used for the tip of bores in the swash zone (e.g., Jiang et al., 2010):

$$u_{crest} = 2\ (g\ h_c)^{0.5} \qquad (2)$$

Where u_{crest} is the overwash leading edge velocity (m s^{-1}), g is acceleration due to gravity (m s^{-2}) and h_c is the overwash water depth (m). Additionally, empirical forms of equation 2 based on laboratory or field data are available. For example, Holland et al. (1991) used field data from video to obtain an empirical expression to relate overwash depth and velocity:

$$u_{crest} = 2.6\ (g\ h_c)^{0.5} \qquad (3)$$

A similar result was obtained by Donnelly (2008) using laboratory and field data (including Holland et al., 1991):

$$u_{crest} = 1.53\ (g\ h_c)^{0.5} \qquad (4)$$

The same type of power fitting model was applied to BARDEX data, and a relation was obtained (Figure 5a):

$$u_{crest} = 2.35\ (g\ h_c)^{0.5} \qquad (5)$$

The curve adjustment using equation 5 had $R^2 = 0.52$ and RMSE = 1.32 ms^{-1}. The constant of proportionality varies between the equations, with the coefficient obtained using BARDEX data (2.35; equation 5) comparable to the result of Holland et al. (2.6; equation 3) and the analytical approach (2; equation 2). The same approach was used to analyse the relation between depth and velocity, but using the velocity obtained with the continuity method (Figure 5b). The obtained coefficient was smaller (1.86), closer to the one obtained by Donnelly (1.53; equation 4). It should be pointed out that differences between coefficients are expected as BARDEX experimental data covers a wider range of overwash leading edge velocities (Figure 5) than other data-sets, but overwash depths were always shallower than 0.8 m (Figure 2).

4.3. Overwash discharge

For the computation of overwash discharge over the crest, the depth-averaged velocities (continuity velocities) were deemed more suitable, as explained previously. The majority of individual overwash discharges recorded in all runs were < 2 m^3 m^{-1}, but maximum individual overwash discharge was about 6 m^3 m^{-1} (Figure 6). The average individual discharge rate computed over the duration of the 15-min test runs was very similar for all three runs: 0.31 m^3 m^{-1} s^{-1}, 0.35 m^3 m^{-1} s^{-1} and 0.31 m^3 m^{-1} s^{-1}. Overall, the total overwash discharge into the lagoon during the 15-min runs E10A, E10B and E10C was 55 m^3 m^{-1}, 62 m^3 m^{-1} and 67 m^3 m^{-1}, respectively. The increased discharge from E10A to E10C is in line with the increase in overwash potential related to crest lowering discussed previously, and an associated increase in total overwash duration from 177 seconds of overwash over the barrier crest in E10A to 215 seconds in E10C.

BARDEX overwash discharges over the barrier crest are high when compared to safety standards for coastal engineering structures (e.g., Pullen et al., 2007). With overtopping/overwash water discharge over the crest of a structure/barrier higher than 0.05 $m^3 m^{-1} s^{-1}$ or a single overtop volume of water higher than 1 $m^3 m^{-1}$, no pedestrians or vehicles would safely pass behind the barrier, even at low speed. A relatively low wave energy was simulated during Test Series E10 of BARDEX experiment (H_s = 0.8 m), when compared with wave energy during overwash of gravel barriers, when storm wave height may be 3.5 m (Hurst Spit, U.K., Bradbury and Powell, 1992), 3.5 m (Carnsore, Ireland, Orford and Carter, 1984), 4 m (Rialto Beach, U.S.A., McKay and Terich, 1992), 4 m (Slapton Sands, U.K., Alegria-Arzaburu and Masselink, 2010), 5 m (Porlock Barrier, U.K., Orford et al., 2003), 6.5 m (Chesil Beach, U.K., May and Hansom, 2003). Assuming that equations 2 to 5 are valid approaches, then overwash velocity at crest is solely dependent on the overwash depth, and therefore *OP* at the crest. In nature, barrier crest elevation is defined by the distribution of wave runup as a function of breaker height, beach slope and bed roughness (Orford et al., 2002). Barrier elevation also reflects a balance between runup sufficient to deposit material at the beach crest (overtop) and runup sufficient to exceed the crest and move sediments onto the backbarrier slope (overwash). The combination that is required to produce positive values of *OP* is therefore site-specific, requiring either a low-lying barrier with moderate wave energy at one end of the scale, or a high-elevation barrier during extreme storms, at the other. For both situations, individual overwash discharges may be similar to the ones measured during the BARDEX experiments given that *OP* values are similar. However, overwash frequency during the event may be different as it is also related to wave period, and therefore the total volume of water that passes the barrier crest during the whole overwash event may vary greatly.

5. OVERWASH FROM A LAGRANGIAN PERSPECTIVE

5.1. Overwash depth across the barrier

Overwash depth across the barrier varied significantly, both within each overwash event and from one event to another. Maximum depths were recorded at the barrier crest, but the depth decrease across the backbarrier varied from event to event. As an example, Figure 3 shows overwash events 12, 13 and 14 at the backbarrier, during E10B. The three events had similar durations over the crest, (4.00 s to 4.25 s), but event 13 was clearly the largest, with 46 cm water depth at the crest. Events 12 and 14 had depths of 19 cm and 18 cm at the crest, respectively. Event 12 reached the lagoon, but event 14 did not. Overwash velocities at the crest for events 12 and 14 were 3.2 m s^{-1} and 3.0 m s^{-1}, respectively. Therefore, the overwash progression at the backbarrier is sensitive to small variations in the combination of hydrodynamic and morphological factors at the crest. This includes variations in sediment properties across the backbarrier that influence the infiltration rate, and therefore the progression into the lagoon.

Considering all overwash events from the three runs (E10A, B and C), the peak average depth over the crest is 21 cm, at the backbarrier slope break is 12 cm, and at the steep slope, before the lagoon, is 9 cm. To gain a more integrated perspective of the overwash at the backbarrier, an average overwash peak depth profile was produced (Figure 7a). Only overwash events that reach the lagoon were used for this profile, so that there is a depth record for all sensors. Overwash flow across the barrier can be divided into 3 sections: at the crest, barrier top and backbarrier steep slope. At the barrier crest there is a sudden 50% decrease in flow depth (37 cm to 19 cm) within the first 1 m (see also Figure 3, event 13) as the flow progresses over the back of the crest and infiltrates into the bed. Over the first 3 m of the barrier top (from $x = 94$ m to 97 m, Figure 7a), mean overwash depth decreases to 12 cm, but across the whole steep backbarrier slope the water depth profile is almost parallel to the barrier profile, with a depth of approximately 10 cm (Figure 7a).

The average overwash flow across the barrier at BARDEX is different from water progression schemes used for overtopping and overwash modelling as shown in Figure 7b (e.g., Schuttrumpf and Oumeraci, 2005). In these simplifications only two sections are generally identified (Schuttrumpf and Oumeraci, 2005; Pullen et al., 2007) and sometimes only one (Nguyen et al., 2006). In these simplified geometric shapes there is no such sharp decrease in flow depth at the crest and also there is a steady depth decrease across the backbarrier.

In the case of overtopping of coastal structures, where the profile is artificially built and the bed is impermeable or consists of large blocks, the overwash profile is different from that recorded during BARDEX. Even in the case of natural gravel barriers, there is a variety of profile morphologies, dimensions, wave exposure, etc. The beach profile used at the BARDEX experiment was based on Slapton Sands, Devon, England (Austin and Masselink, 2006). Many gravel barriers are also narrow with a steep backbarrier (Figure 8), such as Dunwich-Walberswick barrier, Suffolk coast, U.K. (Pye and Blott, 2009) or Miseners Long Beach, Nova Scotia, Canada (Taylor et al., 1997), but others are wider and flatter such as Tacumshin barrier, southeast coast, Ireland (Orford et al., 1988). The average overwash profile measured during BARDEX is not representative of all overwash hydraulic characteristics of all gravel barriers, but it is probably closer to real situations than the simplified schemes from the coastal engineering literature. Probably, wider gravel barriers would have even more or different overwash sections than those identified in the BARDEX case, for example pouding in small depressions, or alongshore-directed flow sections induced by irregularities and obstacles on the barrier top morphology.

5.2. Overwash intrusion

The intrusion distance of overwash events beyond the barrier crest was variable between 0.5 m and 9.8 m, when it reached the lagoon water. The longest overwash events were those with greater depths over the crest; conversely, limited intrusion overwash reaches the crest with shallow depths (Figure 9). Discounting those events which reached the lagoon there is a linear relation between overwash depth at the crest and the intrusion distance (Figure 9). The relation is expressed by:

$$h_c = 0.03\ i \qquad (6)$$

where h_c = water depth at the crest and i = intrusion distance in relation to crest. The adjustment expressed in equation 6 has a $R^2 = 0.65$ and a RMSE = 0.05 m, and does not use data from events which reached the lagoon when the intrusion distance > 9.8 m. This relation is useful for coastal management since it provides an estimate of where the overwash may reach inland, and therefore the likely hazard areas. Note that this relation assumes a backbarrier without obstacles, depressions (wet or dry), etc, and is probably sensitive to morphology and sediment grain-size and packing variations. As mentioned earlier, the gravel barrier shape is variable (Figure 8) which influences the intrusion. The distance to the lagoon is certainly one of the most important limiting factors, but also the backbarrier slope, the width of the barrier top, the barrier grain-size and sorting, and the degree of saturation or depth to water table. The influence of these and other variables cannot be determined solely with data from the BARDEX experiment. Future research efforts should focus on providing complimentary data on different barriers.

Intrusion is one of the most important parameters for coastal zone management, particularly in locations with human development on the coast. The safety standards on the coast curtail urban development to beyond maximum overwash intrusion distance for storm conditions of a given return period. Therefore, the availability of a simple and reliable intrusion predictor is significant. Management plans often rely on simple predictive tools rather than sophisticated methods, and the relation obtained here may move us a step further in this research.

5.3. Overwash infiltration

An assessment of the volume of water infiltrating into the back-barrier was obtained by computing the flow volume passing BLS 32 to 45 (Figure 1) during each overwash event, and assuming that any difference in flow volume between adjacent sensors must have been lost due to infiltration into the barrier. Figure 10 shows the variation of the total overwash volume per event with cross-shore location on the back-barrier for the 53 overwash events observed during run E10B. It is observed that for all events, the measured volume decreases in an approximately linear manner with distance landward of the barrier crest. This observation implies that the rate of volume loss within each event is approximately constant as the overwash flows propagate over the back-barrier, though there is some evidence that the rate of volume loss decreases slightly with the flow depth. Assuming a constant rate of volume loss during each event, but a different rate between different events, Figure 11 displays the mean flow volume lost through the barrier during each overwash event per metre length of back-barrier as a function of the peak overwash depth at the barrier crest (BLS32). It is observed that between 0.046 and 0.865 $m^3\ m^{-1}$ width of flow volume is lost per metre of barrier and the volume lost increases strongly with increasing overwash depth. This result is explained by the fact that infiltration rates into the barrier will increase as the head of water increases.

5.4. Overwash-induced bed changes across the barrier

Using data from bed-level sensors (BLS), an event-by-event analysis of local bed level changes is possible. It is acknowledged that sediment flux per event is a more appropriate measure of sediment transport per overwash (Blenkinsopp et al., 2011); however, as overwash events cause sediment to be transported into the lagoon where it cannot be measured by the BLS, such estimates were not possible. There are three main areas of sub-aerial barrier changes due to overwash, each represented in the following description by changes recorded by particular bed-level sensors: the crest (BLS 32; Figure 1), the barrier top (BLS 38) and the backbarrier region before the lagoon (BLS 42). Figure 12a shows the cumulative bed-level variation throughout E10A until E10C for the three selected locations. As mentioned, BLS32 and BLS38 sites experienced net erosion (26 cm and 14 cm, respectively) and BLS 42 experienced net accretion (11 cm) and was also characterised by the largest individual bed level changes (Figure 12b). However, it is noted that the bed variations induced by the overwash flows were not always in the same direction for each site; rather, a high number of very small positive or negative bed changes were recorded, mostly in the range ± 2 cm (Figure 12b). These positive (accretion) and negative (erosion) changes tended to almost balance out over the duration of each test leading to extremely small average bed changes per overwash event given the roughness of gravel bed: -1.6 mm, -1.5 mm, and 1.9 mm, respectively for BLS32, BLS38, and BLS42. Surprisingly, the landward site (BLS42) recorded the highest positive and negative changes per event, despite the fact that overwash flow velocities were smallest at this location (Figure 12d). According to data presented in this study, there is no apparent direct relationship between the overwash flow velocity and the magnitude of local morphological change (Figure 12c). Overall erosion at BLS32 and BLS38 occurred due to a slightly higher number of erosive than accretionary events (Figure 12b). For the three analysed cross-shore locations, the average positive and negative bed level changes were almost equal, i.e. for BLS32 the average accretionary overwash promoted an 8 mm bed raise while the average erosive overwash promoted an 8 mm bed lowering. For BLS 38, average accretion and erosion were 7 mm and 8 mm, respectively; and for BLS42, average accretion and erosion were 20 mm and 25 mm respectively. Therefore, the overall morphological variation at each location is mostly dependent on the number of events that promote erosion/accretion. For BLS32 and BLS38, 57% of events promoted erosion leading to an overall lowering of the bed at these locations, whereas for BLS42, 59% of events caused increases in bed elevation leading to net accretion.

Results from the event-by-event analysis reveal that net morphological changes result from slight variations in the proportion of accretionary and erosive events, since mean changes per event are very similar. This is probably because at the barrier top (where sensors 32 to 42 are located, Figure 1) the sediments are in a section of their total transport path from the beach to the distal backbarrier. For each overwash event, there is an almost even balance of sediments arriving and leaving that position, i.e. at each location the amount of sediment arriving due to the incoming flow is only slightly different from the amount of sediment leaving due to the outgoing flow. Figure 1e indicates how regular this process is, with similar total changes over the barrier as a whole occurring during each of runs E10A, E10B and E10C. It is suggested that the more energetic overwash flows transport a relatively large amount of sediment to each location, but simultaneously erode more sediment from that site, and vice-versa, indicating why bed changes appear to be independent from overwash velocity.

From the results presented here, it seems that prediction of bed changes at each location cannot be done in a deterministic way, since similar flows promote different bed variations. Rather, the overall morphological variation result from a slight imbalance balance between the percentages of erosive/accretionary events, i.e. net accretion/erosion occurs when more than 50% of overwash flows induce erosive/accretionary bed changes. Therefore, an important factor to predict morphological changes is the correct location of the nodal point, seaward of which flows have an erosive balance and landward of each more than 50% of flows induce accretion. For the BARDEX barrier, the nodal point is located around BLS40, a significant distance (5–7 m) landward of the barrier crest (Figure 1e). This distance corresponds to the location of the average overwash flow intrusion distance for all runs analysed here (6 m from the barrier crest; Figure 9). Average intrusion can be determined from equation 6, given the average depth over the crest, which can be measured or predicted by the computation of the overwash potential (*OP*, equation 1 of section 3).

6. CONCLUSIONS

The paper provides the first measurements of hydrodynamic and morphological evolution of a gravel barrier during overwash at proto-type scale. The observed morphological evolution of the barrier reveals a net erosion of the beach and barrier crest, with sediments transported to the back-barrier region and deposited both in the sub-aerial and submerged part of the barrier lagoon margin. An event-by-event analysis of bed changes shows that the barrier top is part of an onshore transport path under intermittent and variable overwash flows that either erode/accrete sediments on their way to the steep backbarrier slope that is mostly accreting.

It is observed that from test Series E10A to E10C, the overwash frequency increases, maximum overwash depth increases (with approximately 50% of waves generating overwash flows), and depth curves become more symmetrical resembling propagating waves. Mean overwash velocities at the barrier crest were relatively high (around 3 m s^{-1}) as well as the total overwash discharge into the lagoon. Considering safety standards for coastal engineering structures, these overwash volumes would imply that no pedestrians or vehicles would safely pass behind the barrier, even with relatively low wave energy simulated during BARDEX ($H_s = 0.8$ m).

According to data collected during this study, overwash flow across the barrier can be divided into 3 sections: at the crest (where overwash flow depth show a sudden decrease), barrier top (with a smaller reduction in overwash depth) and backbarrier steep slope (where the depth is relatively constant). This depth profile is different from water progression schemes used for overtopping and overwash modelling.

Two relations are obtained: one that relates peak overwash depth at the barrier crest to velocity at the crest (power fit model); and another that relates peak overwash depth to intrusion distance (linear fit model). It must be stressed that the relations identified in this study are empirical and developed based on laboratory conditions. Nevertheless, relations based on results from flume experiments have been proven to have valuable contributions for real situations, for example, the runup equation of Hunt (1959), and the coarse grained profile model detailed by Van der Meer (1988). Data from other experiments, and most importantly from fieldwork are essential to verify the range of applicability of these relations, perhaps augmented by numerical modelling. A lack of published data on the hydraulics of overwash over gravel barriers does not allow such an evaluation to be done within this study.

Results presented in this study provide a valuable insight of overwash on gravel barriers and a detail analysis of processes in an event-by-event scale. Results should be used with care since field and laboratory situations are different;

however, given the technical difficulty and hazard of undertaking fieldwork during overwash in gravel barriers, the obtained datasets are unique and useful to improve models of barrier overwash and breaching.

Acknowledgements

The data reported here were collected in the Delta flume (The Netherlands) as part of the EU-funded BARDEX project (HYDRALAB III Contract no. 022441 (RII3), Barrier Dynamics Experiment). Ana Matias was supported by the RUSH Project (From Runup to Overwash, reference PTDC/CTE-GIX/116814/2010) and Gerd Masselink was supported by the NUPSIG project (New Understanding and Prediction of Storm Impacts on Gravel Beaches) funded by the EPSRC (reference EP/H040056/1) We would like to thank all BARDEX collaborators for their contributions, but in particular those who participated in overwash experiments: Celia Swinkels, Daniel Buscombe, Rita Carrasco, Amaia Alegria-Arzaburu, and Saul Reynolds.

References

Alegria-Arzaburu, A. R., and Masselink, G. (2010). Storm response and beach rotation on a gravel beach, Slapton Sands, U.K. Marine Geology 278, 77-99.

Alessandro, F., Fortes, C. J., Ilic, S., James, M., Sancho, F., Schüttrumpf, H., and Tomasicchio, G. R. (2010). Wave storm induced erosion and overwash in large-scale flume experiments. Proceedings of the HYDRALAB III Joint User Meeting. Hannover, Germany.

Austin, M. J., and Masselink, G. (2006). Observations of morphological change and sediment transport on a steep gravel beach. Marine Geology 229, 59-77.

Baldock, T. E., Hughes, M. G., Day, K., and Louys, J. (2005). Swash overtopping and sediment overwash on a truncated beach. Coastal Engineering 52, 633-645.

Blenkinsopp, C., Turner, I., Masselink, G., and Russel, P. (2010). Validation of volume continuity method for estimation of cross-shore swash flow velocity. Coastal Engineering 57, 953-958.

Blenkinsopp, C., Turner, I., Masselink, G., and Russel, P. (2011). Swash zone sediment fluxes: field observations. Coastal Engineering 58, 28-44.

Bradbury, A., Cope, S. N., and Prouty, D. B. (2005). Predicting the response of shingle barrier beaches under extreme wave and water level conditions in Southern England. Proceedings of Coastal Dynamics, ASCE, Barcelona, Spain.

Bradbury, A. P., and Powell, K. A. (1992). The short term profile response of shingle spits to storm wave action. Proceedings of International Conference on Coastal Engineering, Venice, Italy, pp. 2694-2707.

Bray, M. J., and Duane, W. (2001). Porlock Bay: geomorphological investigation and monitoring - gravel barrier breaching and tidal lagoon development. Environment Agency Science Report SC980010/SR, pp. 111.

Bray, T. F., and Carter, C. H. (1992). Physical processes and sedimentary record of a modern, transgressive, lacustrine barrier island. Marine Geology 105, 155-168.

Buscombe, D., and Masselink, G. (2006). Concepts in gravel beach dynamics. Earth-Science Reviews 79, 33-52.

Carter, R. W. G., and Orford, J. D. (1993). The morphodynamics of coarse clastic beaches and barriers: a short term and long term perspective. Journal of Coastal Research SI 15, 158-179.

Cleary, W. J., McLeod, M. A., Rauscher, M. A., Johnston, M. K., and Riggs, S. R. (2001). Beach nourishment on hurricane impacted barriers in Southeastern North Carolina, USA: Targeting shoreface and tidal inlets sand resources. Journal of Coastal Research SI 34, 232-255.

Donnelly, C. (2008). Coastal overwash: processes and modelling. Lund University, Sweden, 53 pp + papers.

Figlus, J., Kobayashi, N., Gralher, C., and Iranzo, V. (2011). Wave overtopping and overwash of dunes. Journal of Waterway, Port, Coastal, and Ocean Engineering, 137, 26-33.

Fritz, H.M., Phillips, D.A., Okayasu, A., Shimozono, T., Liu, H., Mohammed, F., Skanavis, V., Synolakis, C.E., Takahashi, T. (2012). The 2011 Japan tsunami current velocity measurements from survivor videos at Kesennuma Bay using LiDAR. Geophysical Research Letters, 39, L00G23.

Guillén, J., Camp, J., and Palanques, A. (1994). Short-time evolution of a microtidal barrier - lagoon system affected by storm and overwashing: the Trabucador Bar (Ebro Delta, NW Mediterranean). Zeitschrift fur Geomorphologie 38, 267-281.

Hancock, M. W., and Kobayashi, N. (1994). Wave overtopping and sediment transport over dunes. Proceedings of 24th Conference on Coastal Engineering, ASCE, Kobe, Japan, pp. 2028-2042.

Hart, D. E. (2007). River mouth lagoon dynamics on mixed sand and gravel barrier coasts. Journal of Coastal Research, 927-931.

Holland, K. T., Holman, R. A., and Sallenger, A. H. (1991). Estimation of overwash bore velocities using video techniques. Proceedings of Coastal Sediments '91, USACE, Seattle, Washington, USA., pp. 489-497.

Hunt, I.A. (1959). Design of seawalls and breakwaters. Journal of the Waterways and Harbors, Division 85(WW3), 123-152.

Jaffe, B., Buckley, M., Richmond, B., Strotz, L., Etienne, S., Clark, K., Watt, S., Gelfenbaum, G., Goff, J. (2011). Flow speed estimated by inverse modelling of sandy sediment deposited by the 29 September 2009 tsunami near Satitoa, east Upolu, Samoa. Earth-Science Reviews, 107, 23-37.

Jiang, A. W., Hughes, M., Cowell, P., Gordon, A., Savioli, J. C., and Ranasinghe, R. (2010). A hybrid model of swash-zone longshore sediment transport on reflective beaches. Proceedings of International Conference on Coastal engineering, Shanghai, China.

Kobayashi, N., Farhadzadeh, A., Melby, J., Johnson, B., and Gravens, M. (2010). Wave overtopping of levees and overwash of dunes. Journal of Coastal Research, 26(5), 888-900.

Leatherman, S. P. (1977). Overwash hydraulics and sediment transport. Proceedings of Coastal Sediments '77, ASCE, Charleston, USA, pp. 135-148.

Leatherman, S. P., and Zaremba, R. E. (1987). Overwash and aeolian processes on a U.S. Northeast coast barrier. Sedimentary Geology 52, 183-206.

Lorang, M. S. (2002). Predicting the crest height of a gravel beach. Geomorphology 48, 87-101.

Masselink, G and Turner, I.L. (2012). Large-scale laboratory investigation into the effect of varying back-barrier lagoon water levels on gravel beach morphology and swash zone sediment transport. . Coastal Engineering, 63, 23-38.

Matias, A., Ferreira, Ó., Vila-Concejo, A., Morris, B., and Dias, J. A. (2010). Short-term morphodynamics of non-storm overwash. Marine Geology 274, 69-84.

Matias, A., Williams, J. J., Masselink, G., and Ferreira, Ó. (2012). Overwash threshold for gravel barriers. Coastal Engineering 63, 48-61.

Matsutomi, H., Okamoto, K., and Harada, K. (2010). Inundation flow velocity of tsunami on land and its practical use. Proceedings of International Conference on Coastal engineering, Shanghai, China.May, V.J. and Hansom, J.D. (2003). Coastal Geomorphology of Great Britain. Geological Conservation Review Series, No. 28, Joint Nature Conservation Comittee, Peterborough, 754 pp.

McKay, P. J., and Terich, T. A. (1992). Gravel barrier morphology: Olympic National Park, Washington State, USA. Journal of Coastal Research 8, 813-829.

Nguyen, X. T., Donnelly, C., and Larson, M. (2006). A new empirical formula for coastal overwash volume. Proceedings of Vietnam-Japan Estuary Workshop 2006, Hanoi, Vietnam, pp. 60-65.

Obhrai, C., Powell, K., and Bradbury, A. (2008). A laboratory study of overtopping and breaching of shingle barrier beaches. Proceedings of International Conference on Coastal Engineering, Hannover, Germany, pp. 1497-1508.

Orford, J., and Carter, R. W. G. (1984). Mechanisms to account for the longshore spacing of overwash throats on a coarse clastic barrier in southeast Ireland. Marine Geology 56, 207-226.

Orford, J. D., and Carter, R. W. G. (1982). Crestal overtop and washover sedimentation on a fringing sandy gravel barrier coast, Carnsore Point, Southeast Ireland. Journal of Sedimentary Petrology 52, 265-278.

Orford, J. D., Carter, R. W. G., Forbes, D. L., and Taylor, R. B. (1988). Overwash occurrence consequent on morphodynamic changes following lagoon outlet closure on a coarse clastic barrier. Earth Surface Processes and Landforms 13, 27-35.

Orford, J. D., Carter, R. W. G., Jennings, S. C., and Hinton, A. C. (1995). Processes and timescales by which a coastal gravel-dominated barrier responds geomorphologically to sea-level rise: Story Head Barrier, Nova Scotia. Earth Surface Processes and Landforms 20, 21-37.

Orford, J. D., Cooper, J. A. G., Jackson, D., Malvarez, G., and White, D. (1999). Extreme storms and thresholds on foredune stripping at Inch Spit, South-West Ireland. Proceedings of Coastal Sediments '99, New York, USA, pp. 1852-1866.

Orford, J. D., Forbes, D. L., and Jennings, S. C. (2002). Organisational controls, typologies and time scales of paraglacial gravel-dominated coastal systems. Geomorphology 48, 51-85.

Orford, J., Jennings, S., and Pethick, J. (2003). Extreme storm effect on gravel-dominated barriers. Proceedings of Coastal Sediments '03, Florida, USA, ASCE, CD-ROM.

Park, Y. H., and Edge, B. L. (2010). An empirical model to estimate overwash. Journal of Coastal Reseach 26, 1157-1167.

Pullen, T., Allsop, N. W. H., Bruce, T., Kortenhaus, A., Schuttrumpf, H., and Van der Meer, J. W. (2007). Wave overtopping of sea defences and related structures: assessment manual. EurOtop. Die Küste, 73. 178 pp.

Pye, K., and Blott, S. J. (2009). Progressive breakdown of gravel-dominated coastal barrier, Dunwich-Walberswick, Suffolk, U.K.: processes and implications. Journal of Coastal Reseach 25, 589-602.

Rodríguez, R. W., Webb, R. M. T., and Bush, D. M. (1994). Another look at the impact of Hurricane Hugo on the shelf and coastal resources of Puerto Rico, USA. Journal of Coastal Research 10, 278-296.

Schüttrumpf, H., and Oumeraci, H. (2005). Layer thicknesses and velocities of wave overtopping flow at seadikes. Coastal Engineering 52, 473-495.

Shen, M. C., and Meyer, R. E. (1963). Climb of a bore on a beach. Part 3. Runup. Journal of Fluid Mechanics 16, 113-125.

Srinivas, R., Dean, R. G., and Parchure, T. M. (1992). Barrier island erosion and overwash study - Volume 1. Coastal and Ocean Engineering Department, University of Florida, 92 pp.

Stockdon, H.F., Holman, R.A., Howd, P.A., Sallenger, A.H., 2006. Empirical parameterization of setup, swash, and runup. Coastal Engineering, 53, 573-588.

Stone, G., Liu, B., Pepper, D. A., and Wang, P. (2004). The importance of extratropical and tropical cyclones on the short-term evolution of barrier islands along the northern Gulf of Mexico, USA. Marine Geology 210, 63-78.

Taylor, R. B., Forbes, D. L., Frobel, D., Shaw, J., and Parkes, G. (1997). Hurricane Hortense strikes Atlantic Nova Scotia: An examination of beach response and recovery. Geological Survey of Canada, Open File 3503.

Tinh, N. X., Larson, M., Donnelly, C., and Tanaka, H. (2010). Laboratory experiment on cross-shore barrier spit evolution by storm dynamics. Proceedings of International Conference on Coastal Engineering 2010, ASCE, Shanghai, China.

Turner, I. L., Russell, P. E., and Butt, T. (2008). Measurement of wave-by-wave bed-levels in the swash zone. Coastal Engineering 55, 1237-1242.

Van der Meer, J. (1988). Rock slopes and gravel beaches under wave attack. Delft Hydraulics Publications, vol. 396.

Williams, J. J., Buscombe, D., Masselink, G., Turner, I. L., and Swinkels, C. (2012). Barrier dynamics experiment (BARDEX): Aims, design and procedures. Coastal Engineering 63, 3-12.

Figure captions

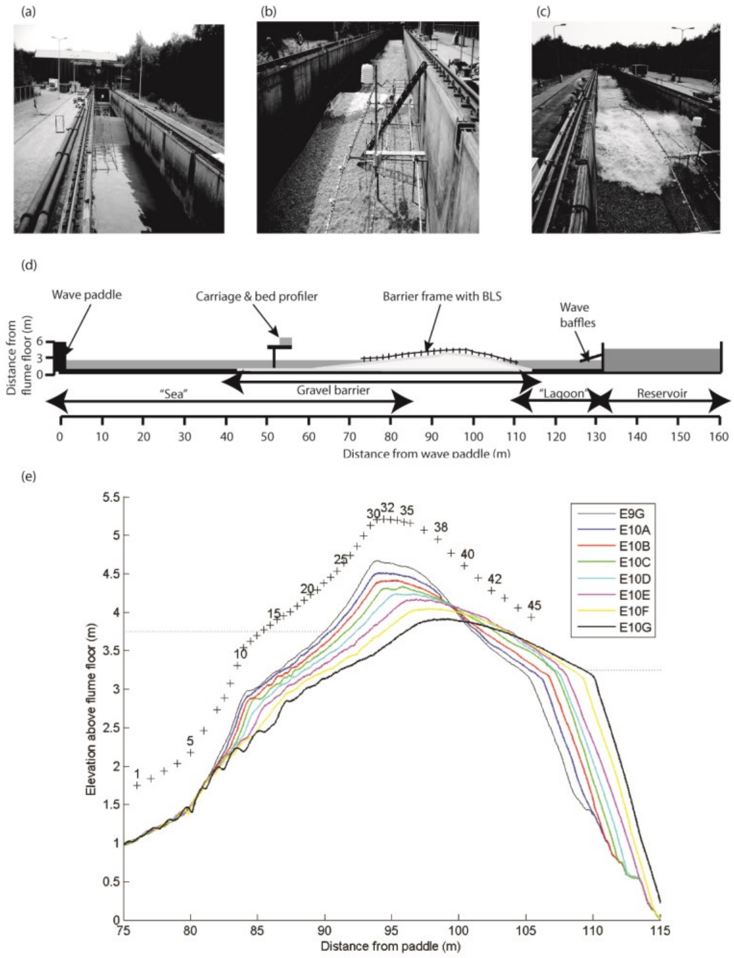

Figure 1. (a) View of the barrier towards the lagoon; (b) View towards the paddle of barrier overtopping; (c) View towards the paddle of barrier overwash; (d) Sketch of the experiment cross-section within the Delta flume; (e) Barrier cross-shore profiles from Test Series , E10A to E10G. Crosses on top of the profiles represent the BLS location and number identification. Water level on the 'sea' side (paddle side, to the left) and 'lagoon' side are also represented in dash-lines.

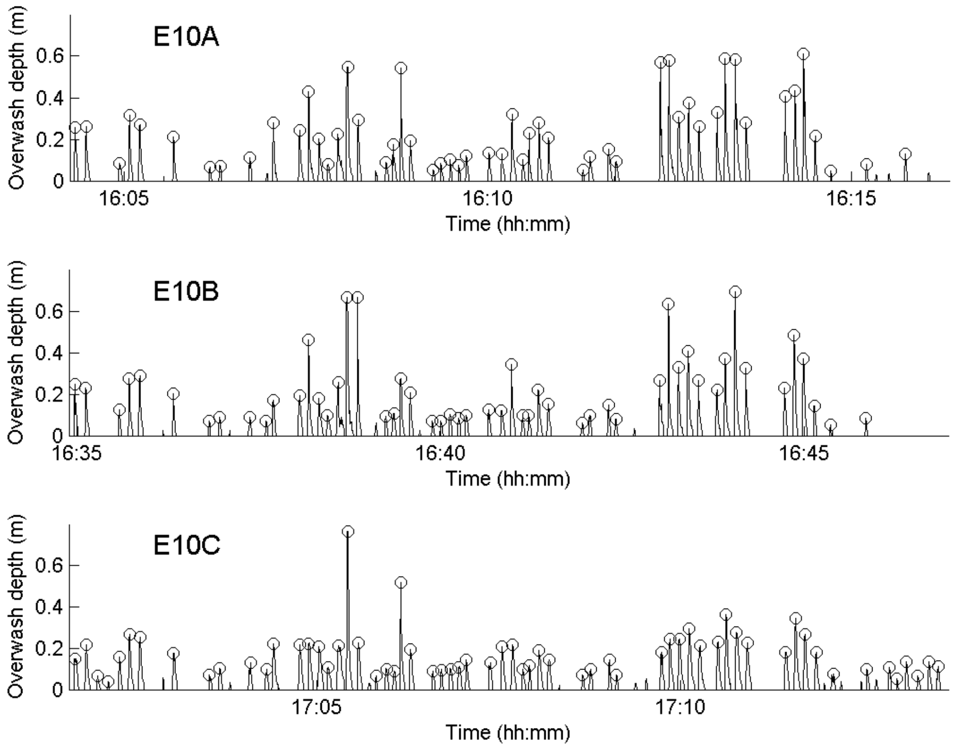

Figure 2. Time-series of extracted overwash depth data recorded during Test Series E10A, E10B and E10C, with the peak depth of each overwash event marked with a circle.

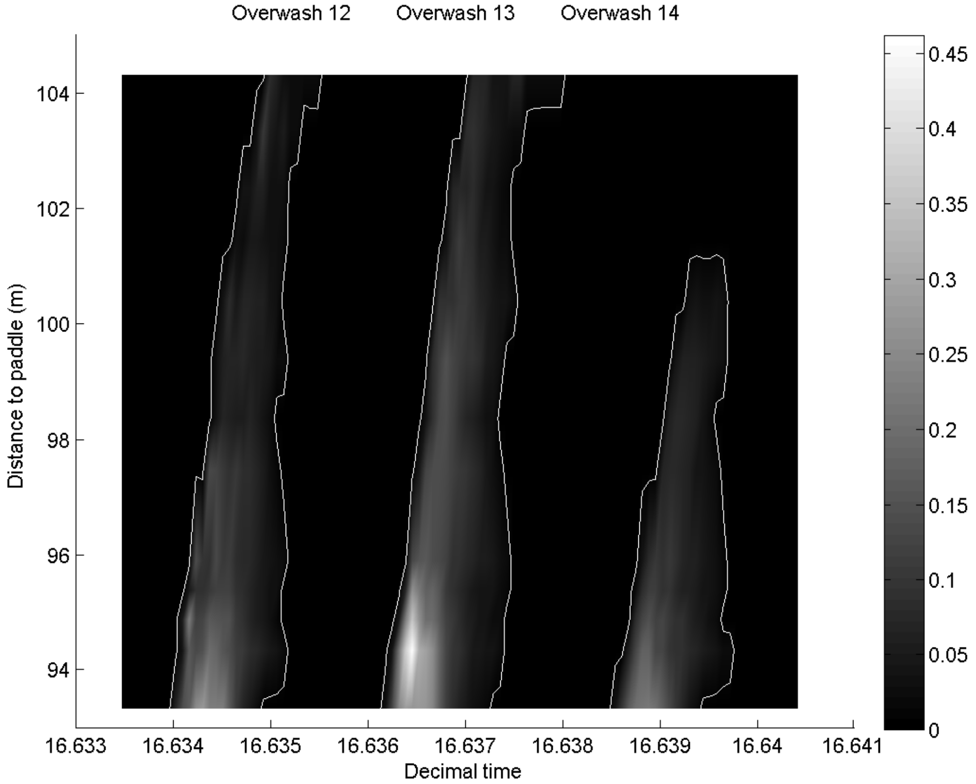

Figure 3. (a) Time-series of the overwash depth over time (xx axis) and across the barrier (yy, lagoon is upwards) for three overwash events (12, 13 and 14, of Test Series E10B).

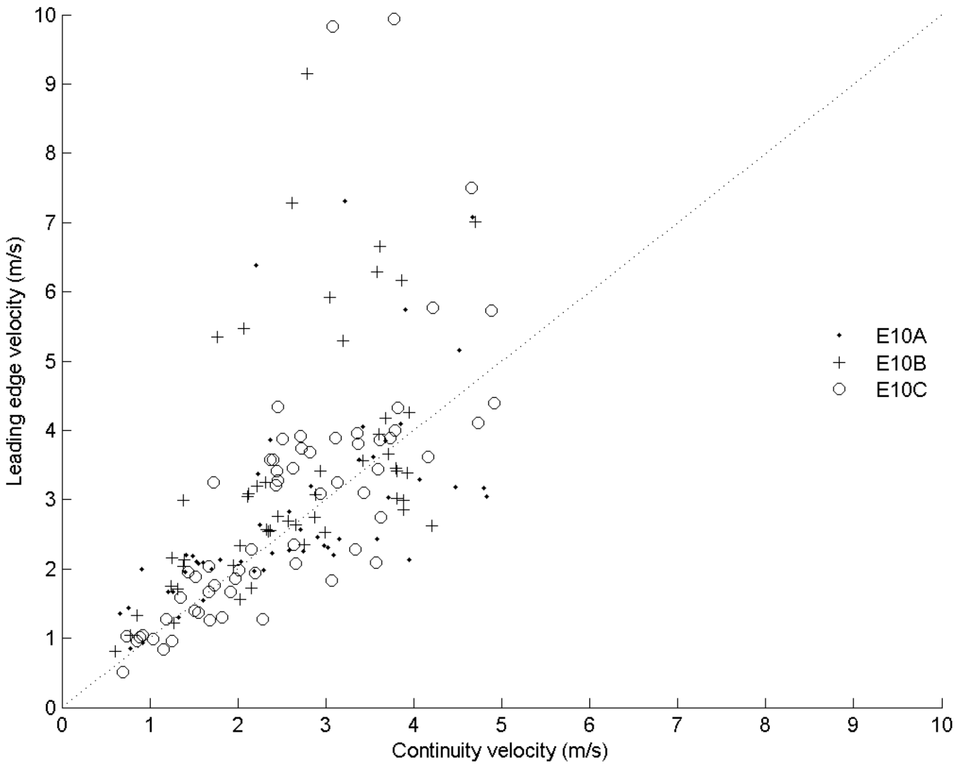

Figure 4. A comparison of velocity estimates using the continuity and leading edge techniques. The equality line is represented with a dashed-line.

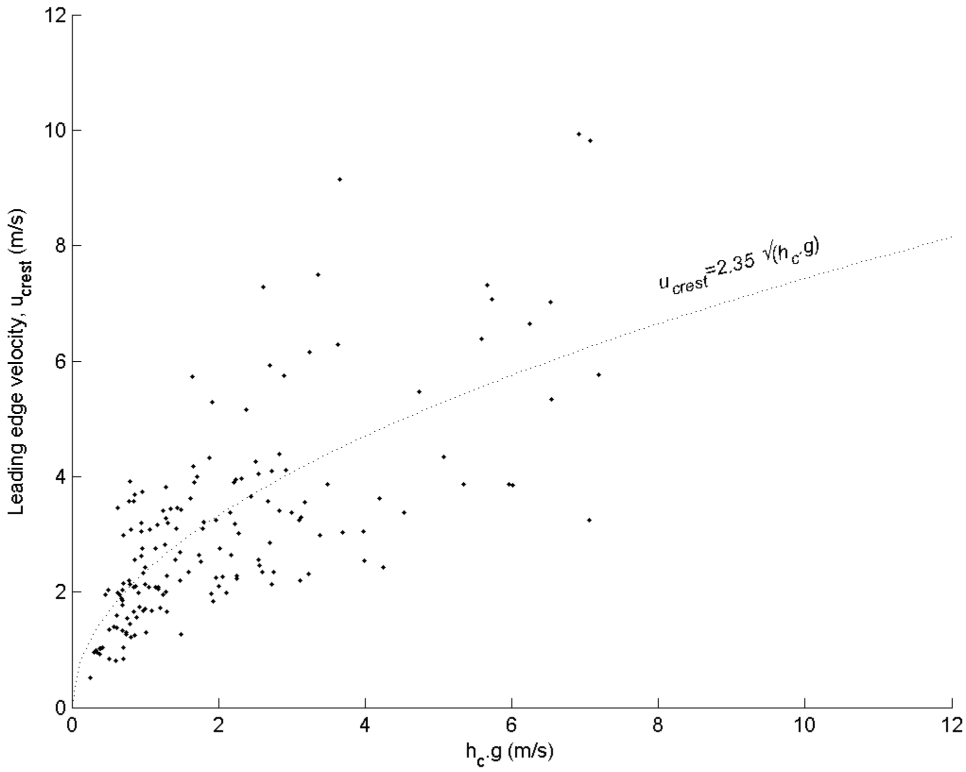
Leading edge velocity, u_{crest} (m/s)
$h_c \cdot g$ (m/s)
$u_{crest}=2.35\ \sqrt{(h_c \cdot g)}$

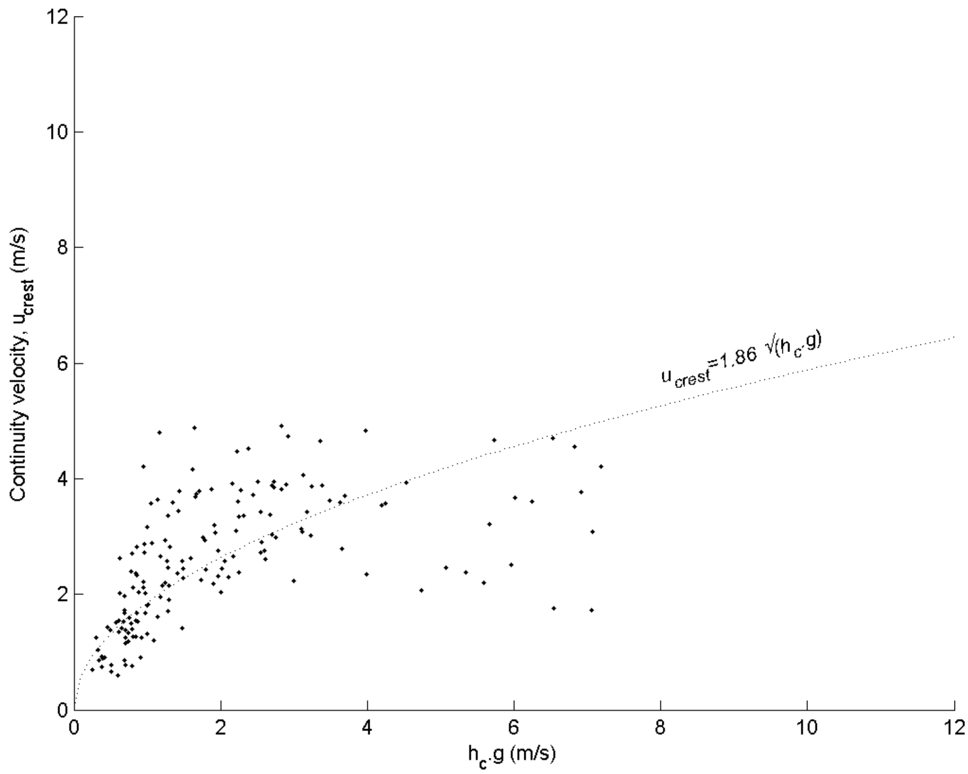
Continuity velocity, u_{crest} (m/s)
$h_c \cdot g$ (m/s)
$u_{crest}=1.86\ \sqrt{(h_c \cdot g)}$

Figure 5. (a) Overwash leading edge velocity at crest (u_{crest}) as a function of overwash depth at the crest (h_c)*gravitational acceleration (g). The line of power fitting adjustment to data is represented with a dashed-line. (b) Overwash continuity velocity at crest (u_{crest}) as a function of overwash depth at the crest (h_c)*gravitational acceleration (g). The line of power fitting adjustment to data is represented with a dashed-line.

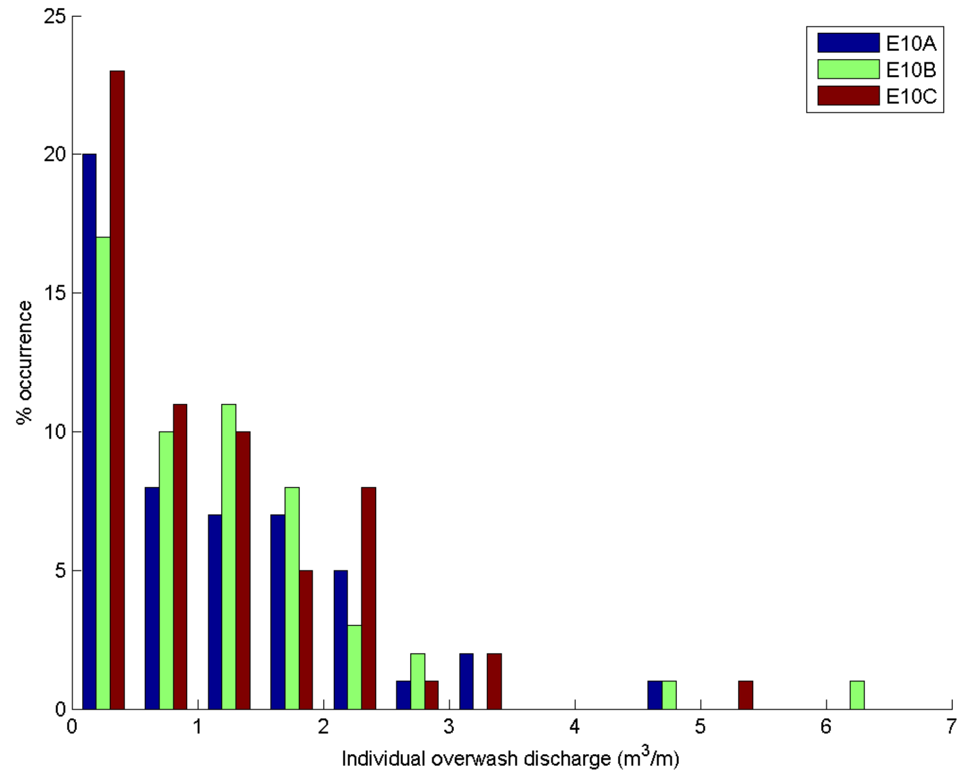

Figure 6. Percentage of occurrence of overwash event discharge over the barrier crest for all events of Test Series E10A, E10B, and E10C.

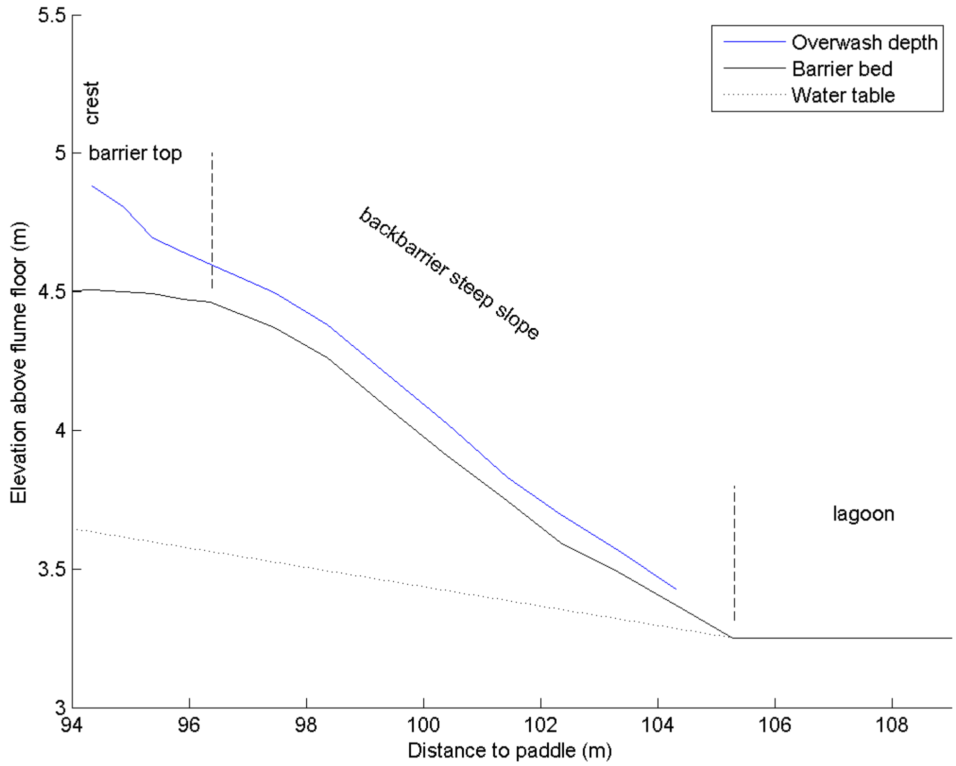

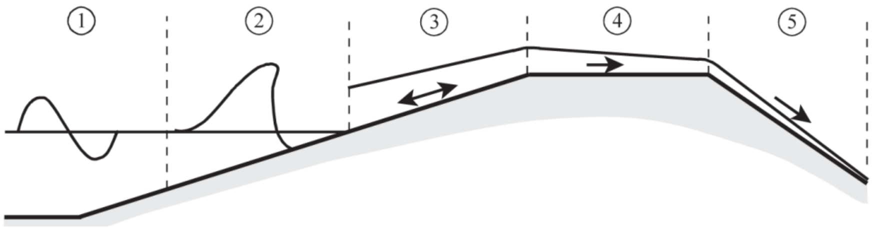

Figure 7. (a) Barrier cross-shore profile from the crest to the lagoon, and mean peak overwash depth across the barrier, considering only overwash events from E10A, E10B and E10C that reached the barrier lagoon edge (BLS 44; 104 m from paddle). (b) Schematic representation of a sea dyke and the flow domains: 1 – toe of the dike; 2 – wave breaking zone of the seaward slope of the dike; 3 – seaward slope of the dike; 4 – dike crest; 5 – landward slope of the dike (from Schüttrumpf and Oumeraci, 2005).

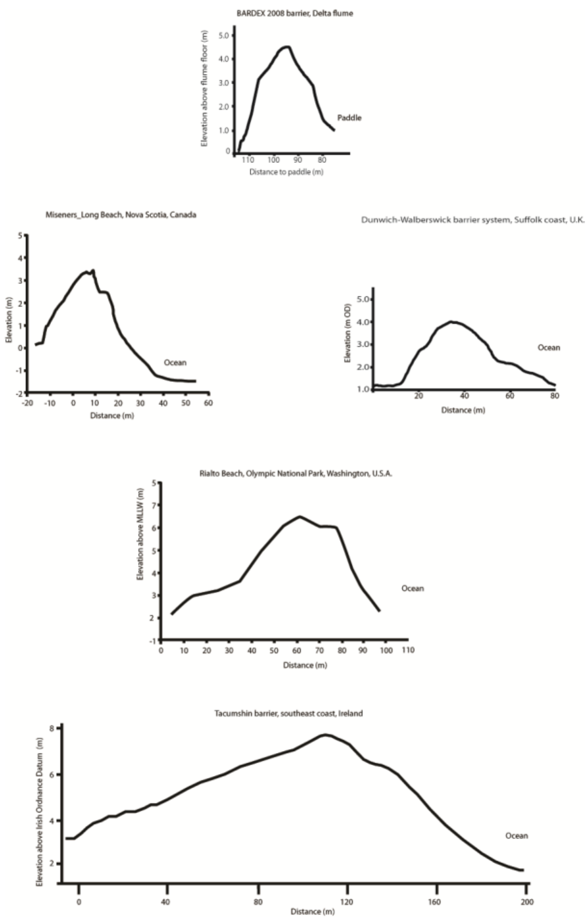

Figure 8. Cross-shore barrier profile from Test Series E10A of BARDEX experiment compared to gravel barrier profiles from several sites: Miseners Long Beach, Nova Scotia, Canada (adapted from Taylor et al., 1997), Dunwich-Walberswick barrier system, Suffolk coast, U.K. (adapted from Pye and Blott, 2009), Rialto Beach, Washington, U.S.A. (adapted from McKay and Terich, 1992); Tacumshin barrier, southeast coast, Ireland (adapted from Orford et al., 1988). All profiles are represented at the same scale.

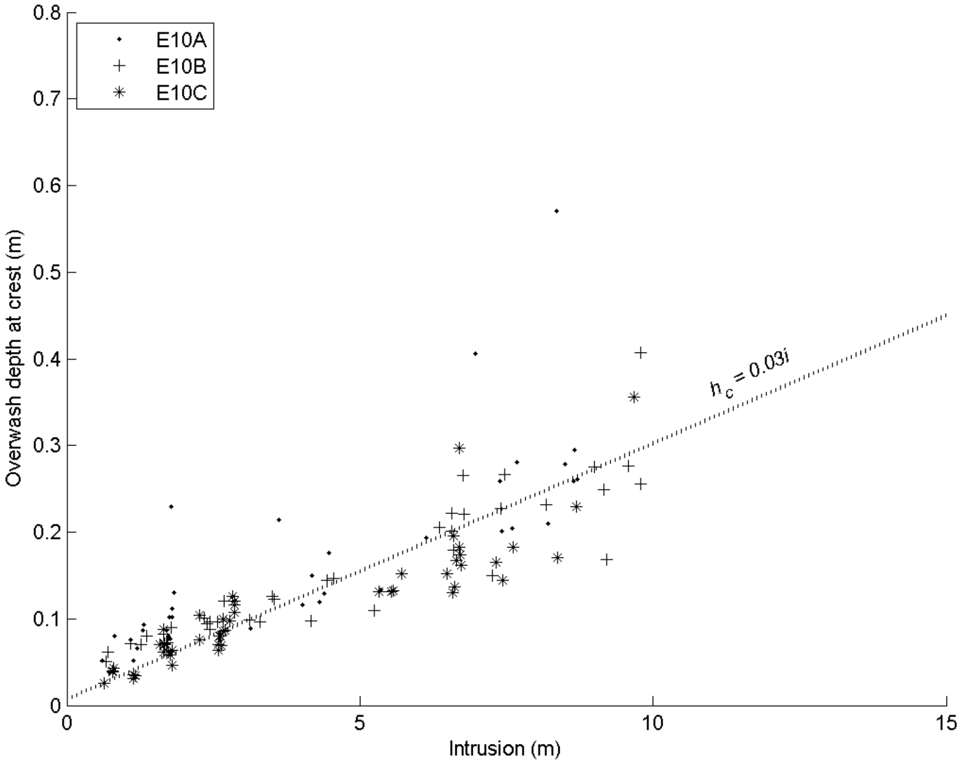

Figure 9. Overwash depth at the crest (h_c)as a function of overwash intrusion (i). A linear fit to the data is represented with a dashed-line. The fitting equation was obtained excluding data with intrusion>9.8 m (distance between the barrier crest and the lagoon).

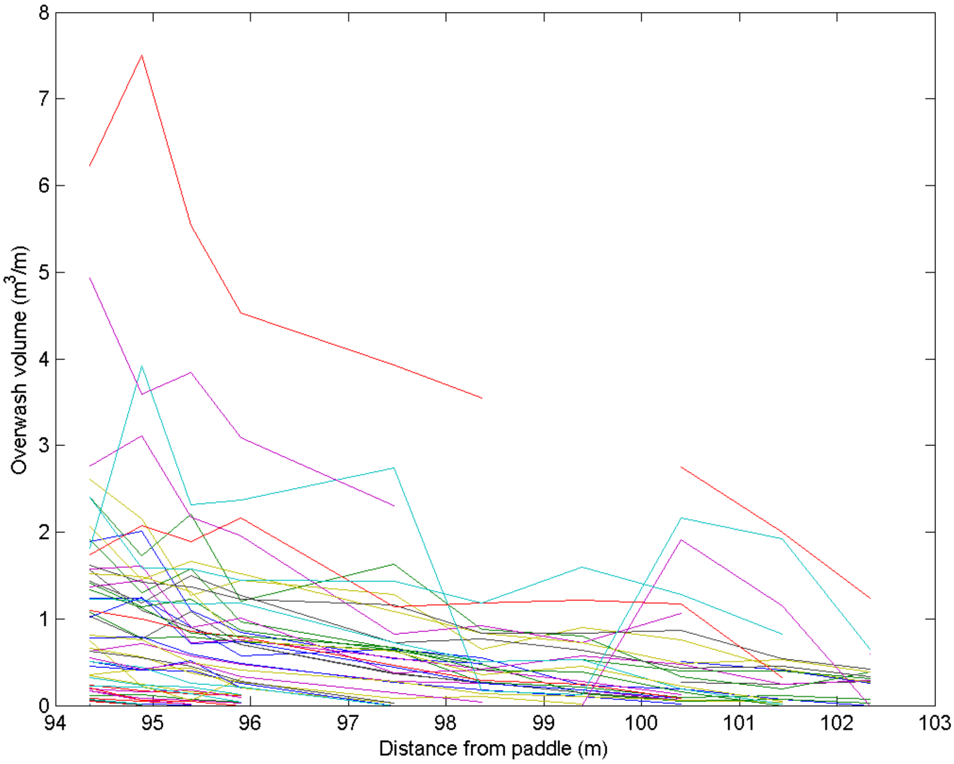

Figure 10. Total overwash flow volume per event across the barrier top and backbarrier, for all overwash events of Test Series E10B.

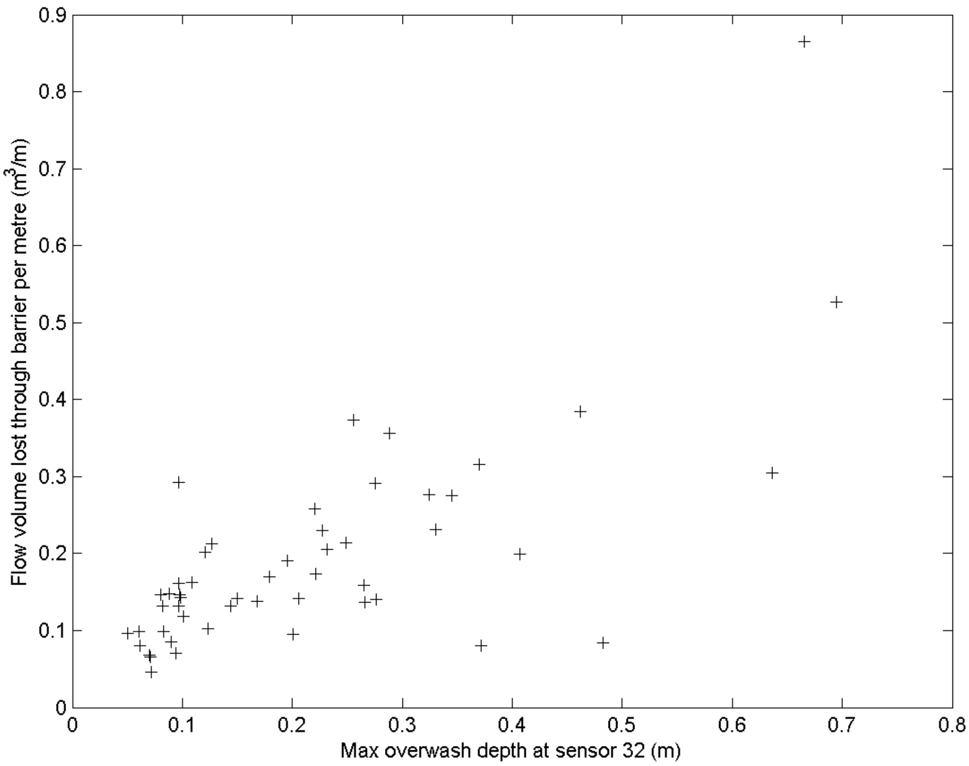

Figure 11. Overwash flow infiltration through the barrier as a function of peak overwash depth at the barrier crest (h_c).

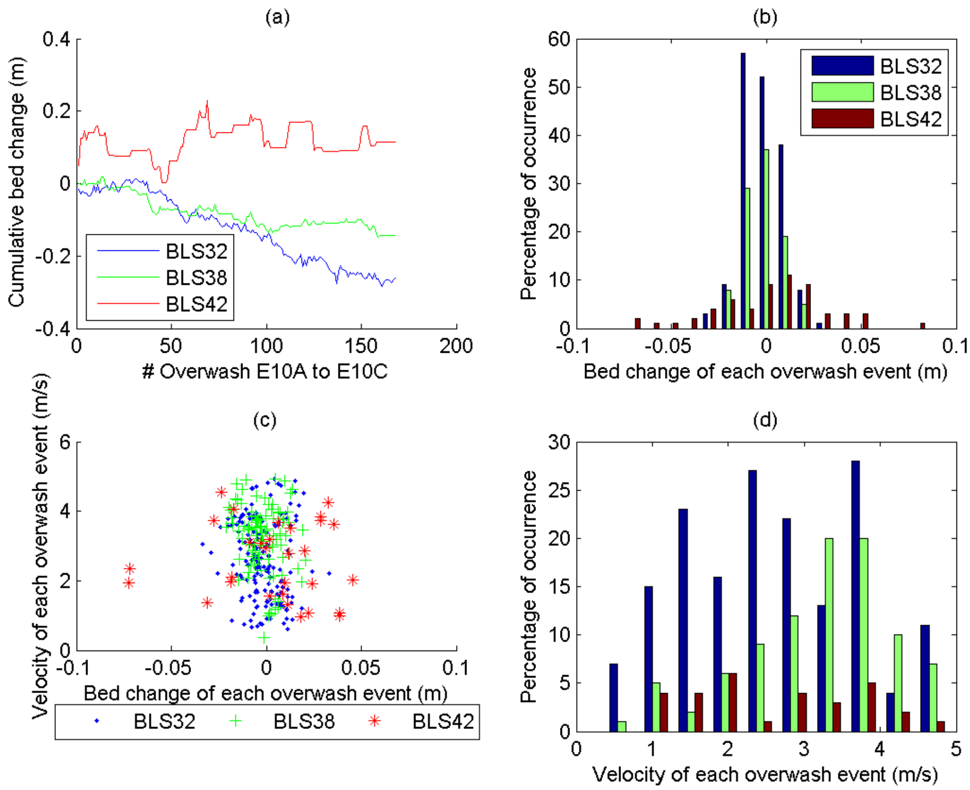

Figure 12. (a) Cumulative bed level change after overwash events from the beginning of E10A until the end of E10C, at the barrier crest (BLS32), barrier top (BLS38) and backbarrier region (BLS42). (b) Percentage of occurrence of bed erosion (negative) and bed accretion (positive) for each overwash event of Test Series E10A, E10B, and E10C. (c) Bed level change versus overwash velocity for every overwash event at the barrier crest (BLS32), at the barrier top (BLS38) and backbarrier region (BLS42). (d) Percentage of occurrence of continuity velocity for all overwash events of Test Series E10A, E10B and E10C.